sustainability

MDPI

Article

Seasonal Responses and Scale Trade-Offs in the Morphological Self-Shading of Guangfu Ancestral Halls: A Case Study of Wanmu Caotang

Yue Pang [1], Yao Xiao [1], Yongyi Ye [2], Li Li [1,*] and Weilong Cao [2]

[1] College of Architecture and Urban Planning, Guangzhou University, Guangzhou 510006, China; pangyue@gzhu.edu.cn (Y.P.); yaoxiao_1104@163.com (Y.X.)
[2] Guangdong Architectural Design and Research Institute Group Co., Ltd., Guangzhou 510010, China; yongyi_ye@foxmail.com (Y.Y.); cwlo@gdadri.com (W.C.)
* Correspondence: lili_ar@gzhu.edu.cn

Abstract

We examined seasonal morphological self-shading using Qiu Clan Study Hall (the former site of Wanmu Caotang), Guangzhou, as a Guangfu ancestral hall prototype. Four hall–courtyard configurations were simulated across 16 orientations in summer and winter. Ecotect and DeST-c were used to calculate the sunlight exposure time ratio (SETR) and mean daily indoor radiative heat gain per room (IRHG), respectively. High values for both indicators generally shifted from easterly and westerly orientations in summer to southerly orientations in winter. Deeper rooms and wider eaves generally corresponded to lower SETR, whereas reference plan area correlated positively with total IRHG ($r = 0.996$ in summer and 0.997 in winter). Shorter direct sunlight exposure could coincide with higher total IRHG, and normalizing IRHG by reference plan area could reverse the heat-gain ranking. With identical adjacent room units, the configuration combining a smaller courtyard footprint and greater enclosure height had lower mean SETR and slightly lower mean IRHG in both seasons. By relating these seasonal solar responses to room and eave dimensions and courtyard enclosure, the study provides quantitative evidence of how a Guangfu ancestral hall prototype regulates indoor solar exposure and heat gain, informing the environmental assessment and adaptive use of heritage buildings.

Keywords: ancestral hall architecture; morphological self-shading; Guangfu architecture; courtyard; seasonal sunlight exposure; indoor radiative heat gain; sustainable heritage conservation; adaptive use

Check for updates

Academic Editors: Fernando Vegas López-Manzanares, Camilla Mileto, Alicia Hueto-Escobar, David Eduardo Morocho Jaramillo and Asterios Bakolas

Received: 23 October 2026
Revised: 19 November 2026
Accepted: 24 November 2026
Published: 27 November 2026

Copyright: © 2026 by the authors. Licensee MDPI, Basel, Switzerland. This article is an open access article distributed under the terms and conditions of the Creative Commons Attribution (CC BY) license.

1. Introduction

The conservation and adaptive use of traditional buildings involve not only preserving architectural forms and historical values but also understanding the environmental performance of existing spaces. Over time, halls, verandas, and courtyards have developed into spatial combinations adapted to local climates [1–7]. Their modulation of sunlight penetration and solar radiation provides an important basis for understanding passive design strategies in traditional architecture [8–10]. In Guangzhou's hot-summer, warm-winter climate, investigating the solar response of these spatial combinations can clarify the relationship between summer sunlight control and winter sunlight access, providing environmental evidence to inform conservation and use.

Studies of climatic adaptation in traditional architecture have examined roof forms, eaves, shading devices, building orientation, and courtyard organization [11–13]. These

studies show that architectural form changes the incidence and obstruction of solar radiation, and that its environmental performance is closely related to spatial dimensions, enclosure, and local climate [10,11]. Courtyards influence sunlight distribution within buildings and are also associated with ventilation and thermal conditions [14,15]. This research provides a foundation for understanding traditional passive design strategies and highlights the need to examine the relationship between form and environmental performance in the context of specific building types and spatial arrangements [2,7].

Courtyard research has examined shading in traditional houses [14], measured thermal conditions in Chinese shophouses [16], and related airflow, microclimate, and spatial organization [15,17,18]. Prior simulations evaluated wind and energy in a two-hall–one-courtyard arrangement [19] or optimized traditional courtyard design [20]. The present study adds a paired comparison in which the hall units are held constant while the courtyard configuration changes. This comparison distinguishes differences in direct sunlight exposure from differences in room-level radiative heat gain across seasons and orientations.

The Guangfu region is centered on the Pearl River Delta (Figure 1a) and experiences hot, humid summers with abundant rainfall. Traditional buildings must address solar exposure while accommodating ventilation and other requirements of use. Previous studies have employed simulation and performance evaluation to investigate building shading [21,22], and have combined in situ measurements with analyses of building thermal conditions and energy demand [23]. Research on traditional Guangfu architecture has addressed the ecological strategies and regional adaptation of bamboo-tube houses [24] and Xiguan mansions [25] (Figure 1b), as well as the inheritance and application of passive heat-protection strategies involving shading, ventilation, and insulation in Lingnan buildings [26]. Recent research has documented the architectural patterns of Guangfu ancestral halls [27]. The present study focuses on how their hall–courtyard configurations relate to seasonal indoor sunlight exposure and radiative heat gain. Guangfu ancestral halls are organized through axes, successive hall units, and bays, with halls, corridors, deep eaves, and courtyards connected in sequence. Indoor sunlight depends on both room geometry and the obstruction provided by neighboring buildings and courtyard enclosure. Their solar response therefore warrants investigation at the level of the continuous hall–courtyard sequence.

In this study, "morphological self-shading" refers to the obstruction of indoor direct sunlight by a building's existing roofs, eaves, walls, and their spatial arrangement. The concept emphasizes the integration of shading with architectural form: eave dimensions modify sunlight penetration, hall depth affects the extent of direct sunlight access, and courtyards together with surrounding buildings create different patterns of spatial obstruction. Because the solar path changes with season and its position relative to the building changes with orientation, the same configuration can exhibit different exposure characteristics. Comparing these differences helps translate environmental knowledge embedded in traditional forms into quantifiable case-based evidence.

The evaluation of morphological self-shading also requires distinguishing what different indicators describe. This study uses two indicators: the sunlight exposure time ratio (SETR), which represents the proportion of the evaluation period during which indoor sampling points receive direct sunlight, averaged across those points; and indoor radiative heat gain (IRHG), which represents the mean daily total radiative heat gain of an entire room. Changes in room geometry may alter both sunlight access and total heat gain, so the two indicators need not follow the same trend. Differences in room area must also be considered when interpreting total heat gain. Here, "scale trade-offs" refer to cases in which lower direct sunlight exposure coincides with higher whole-room heat gain. Heat gain per unit reference plan area is reported as a supplementary comparison to examine whether accounting for room size changes the ranking.

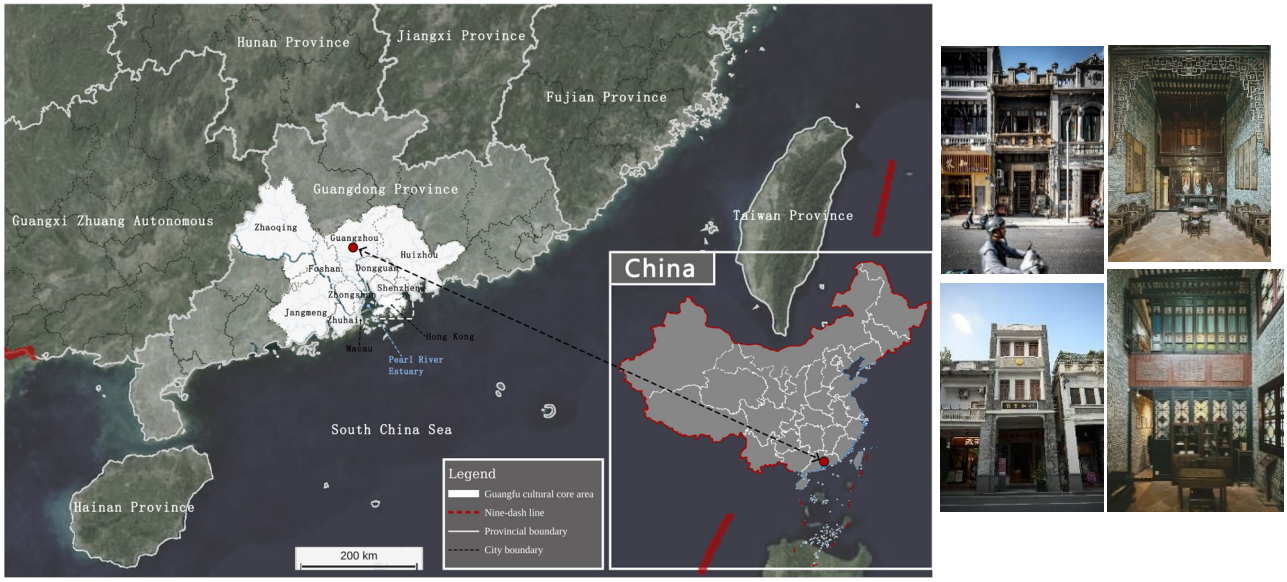

(**a**) (**b**)

Figure 1. (**a**) Location of the Guangfu region; (**b**) Guangfu regional architecture: the tube house and the Xiguan mansion. In panel (**a**), the short red offshore segments on the main map show portions of the nine-dash line depicted in the lower-right inset. This line is used on Chinese maps to depict China's claims in the South China Sea.

From the perspective of sustainable conservation and adaptive use, the environmental value of traditional architectural forms requires explicit performance analysis. Linking regional form, the hall–courtyard sequence, and indoor solar radiation in Guangfu ancestral halls can improve understanding of their climatic response and provide a basis for coordinating future use with environmental improvements. Accordingly, this study develops four spatial configurations based on Qiu Clan Study Hall (the former site of Wanmu Caotang) in Guangzhou and performs summer and winter simulations across 16 orientations using Ecotect and DeST-c. It addresses three questions: (1) What summer–winter differences and orientation patterns characterize indoor direct sunlight and radiative heat gain across configurations? (2) How do room dimensions and eave parameters relate to exposure time and total room heat gain? (3) How does the indoor solar response differ between hall–courtyard configurations, particularly configurations C and D, which use identical room units? The aim is to identify morphological self-shading characteristics and scale trade-offs in this ancestral hall-type prototype, providing case-based evidence for environmental assessment of heritage buildings.

2. Study Object

2.1. Climate of the Guangfu Region

The Guangfu region has a hot-summer, warm-winter climate. Taking Guangzhou, the provincial capital, as an example, Figure 2 summarizes monthly mean maximum, minimum, and average temperatures and precipitation from meteorological records for 1991–2024. Summer extends from May to September and is hot and rainy. July is the hottest month; summer mean maximum temperatures approach 35 °C, while mean minimum temperatures exceed 25 °C. Winter extends from December to February and is mild, with mean maximum temperatures below 20 °C and mean minimum temperatures above 10 °C. Hot weather can occasionally occur in winter.

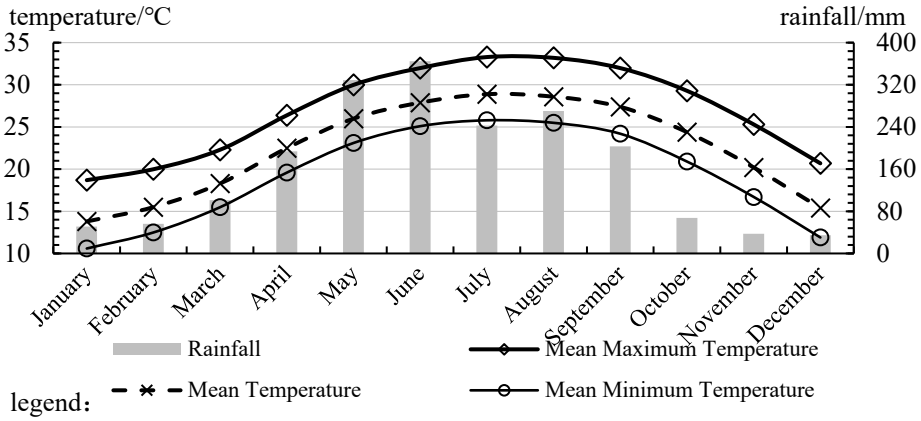

Figure 2. Monthly temperature and precipitation in Guangzhou based on records for 1991–2024 [28].

2.2. Spatial Organization of Guangfu Ancestral Halls

Guangfu ancestral halls combine principal buildings, including the entrance hall (Toumen), central hall (Zhongting), and rear hall (Houzuo), with corridors and courtyards. Their plans can be described through three dimensions: jin, lu, and kaijian. "Jin" denotes successive principal building units along a longitudinal axis (Figure 3a); "lu" denotes longitudinal building sequences arranged side by side (Figure 3b); and "kaijian" denotes structural bays between adjacent column lines across the width of a building (Figure 3c). These concepts describe longitudinal progression, lateral organization, and transverse subdivision, respectively, and together provide a basic framework for expressing ancestral hall layouts [29].

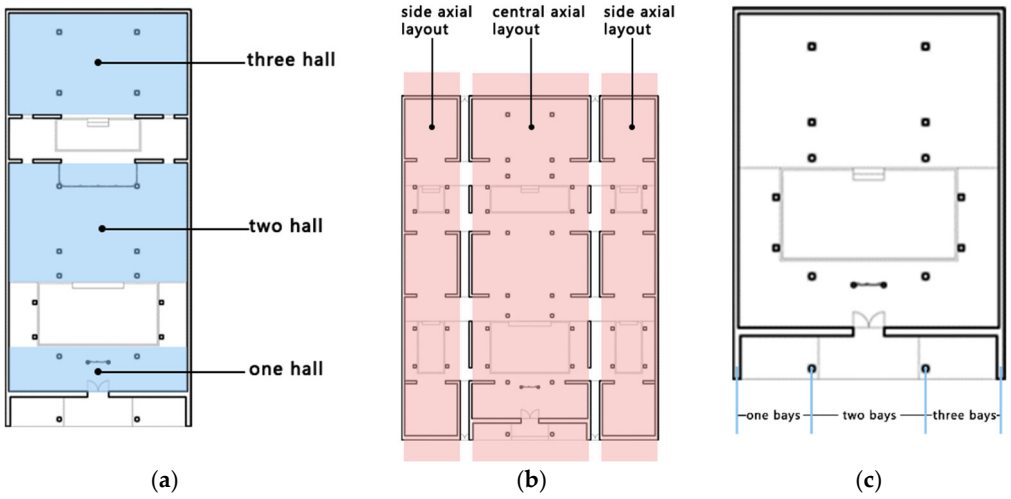

Figure 3. Plan organization of Guangfu ancestral halls. (**a**) Successive hall units ("jin"): one axis, three hall units, and three bays. (**b**) Parallel axes ("lu"): three axes, three hall units, and three bays. (**c**) Structural bays ("kaijian"): one axis, two hall units, and three bays.

In these layouts, halls alternate with courtyards along the longitudinal axis, while corridors connect the front and rear buildings along the sides of the courtyard, forming a continuous hall–courtyard sequence. This study takes a one-axis, two-hall-unit, three-bay arrangement as its basic reference form (Figure 4): two principal building units are aligned longitudinally, with a courtyard between them. The "two hall units" describe longitudinal progression, whereas the "three bays" describe the transverse subdivision of the principal buildings. From this arrangement, a front room–courtyard–rear room combination is

extracted as the basic simulation unit. The principal shading relationships created by the front and rear buildings and the flanking corridors are retained to compare indoor solar responses across room dimensions and courtyard configurations.

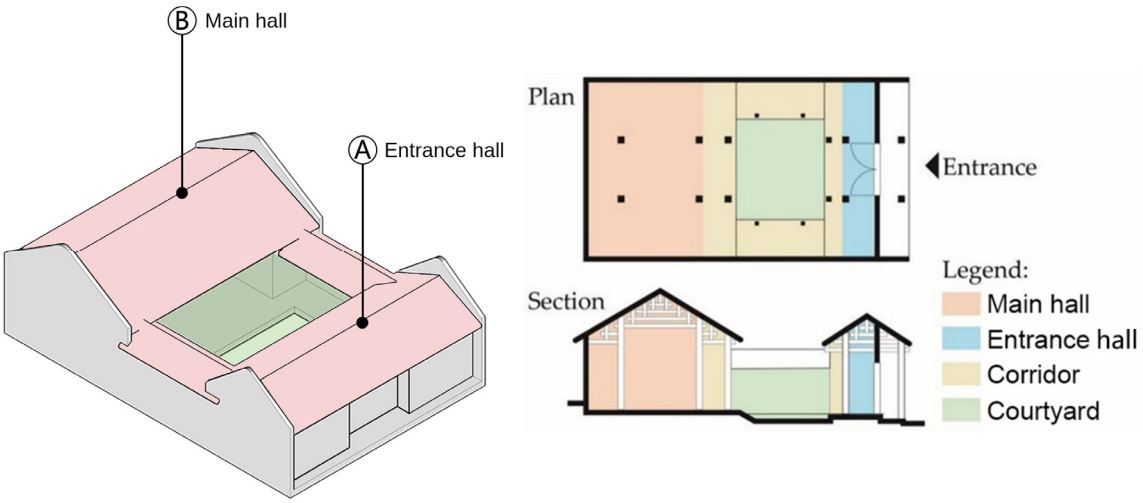

(**a**) (**b**)

Figure 4. One-axis, two-hall-unit, three-bay arrangement: (**a**) axonometric view; (**b**) plan and section.

This arrangement provides the spatial basis for analyzing morphological self-shading in ancestral halls. The dual-pitched roofs, projecting eaves, and walls shown in Figure 4a together define the boundaries that obstruct indoor direct sunlight, while hall depth affects the extent of sunlight penetration. The courtyard provides an opening through which solar radiation can reach the interior of the building complex; the heights, spacing, and relative positions of surrounding buildings jointly determine spatial obstruction. Self-shading therefore needs to be examined in relation to both room geometry and the overall hall–courtyard configuration.

The prototype is Qiu Clan Study Hall (the former site of Wanmu Caotang), Guangzhou, whose principal buildings are organized along one longitudinal axis in a sequence of three hall units and two courtyards. Entrance, hall, and courtyard geometries are extracted from this prototype to develop four configurations based on the one-axis, two-hall-unit, three-bay arrangement. Comparisons of direct sunlight and radiative heat gain among the hall–courtyard combinations reveal seasonal responses of morphological self-shading. Room dimensions and eave parameters are then examined in relation to exposure time and total room heat gain to clarify scale trade-offs between shading of direct sunlight and total room heat gain.

3. Materials and Methods

Ecotect 2011 was used to analyze indoor direct sunlight exposure time, and DeST-c (version 2.0) [30,31] was used to calculate indoor radiative heat gain per room. Models were constructed from the room and courtyard dimensions of Qiu Clan Study Hall (the former site of Wanmu Caotang). This study reports solar-related simulation results under the specified input conditions and interprets their relevance to traditional architecture through spatial form and evaluation scale.

3.1. Evaluation Indicators

To distinguish the obstruction of direct sunlight from the solar-related heat gained by rooms, this study uses SETR and IRHG as its principal indicators. They describe the

exposure time ratio at sampling points and the total radiative heat gain of an entire room, respectively, and are used to compare sunlight exclusion and heat gain across spatial forms.

(1) SETR: The direct sunlight exposure time at each indoor sampling point is first determined within a common evaluation period. The mean exposure time across points is then divided by the duration of that period, as shown in Equation (1).

$$\mathrm{SETR} = \frac{1}{n}\sum_{i=1}^{n} t_i \,/\, t_{day} \times 100\% \quad (1)$$

A lower SETR indicates a shorter direct sunlight exposure time across the specified sampling points and evaluation period. In Equation (1), t_i is the duration of direct sunlight exposure at point i, t_day is the length of the daytime evaluation period, and n is the number of sampling points. Reduced summer exposure generally helps control sunlight penetration; whether greater winter exposure is beneficial also depends on building use and indoor temperature.

(2) IRHG: Under the simulation settings, solar-related room heat gain includes solar radiation transmitted directly through the building envelope and heat transferred inward through convection and heat exchange after absorption by the envelope. The mean daily total heat gain per room for each season is compared in kWh/d. This combined measure was used to account for both transmitted solar radiation and the inward transfer of heat absorbed by the envelope.

$$\mathrm{IRHG} = \frac{Q}{d} \quad (2)$$

IRHG is calculated by dividing the total solar-related indoor heat gain over a season, Q, by the number of days in that season, d, as shown in Equation (2). It is not equivalent to air-conditioning electricity consumption and cannot independently establish indoor thermal comfort. For larger rooms, higher total heat gain may partly reflect larger spatial and building-envelope surface area. For the supplementary comparison, IRHG was divided by the reference plan area (the surveyed reference width multiplied by depth in Table 1) and reported in kWh/(m^2·d).

Table 1. The dimensions of the room in each building block of "Wanmu Caotang".

Category	Element Name	Width (W)	Depth (D)	Eave or Enclosure Height (CH)	Eave Projection Width (CW)	Schematic Diagram of Dimensions
Building Blocks	Toumen	4.800	4.085	4.400	0.630	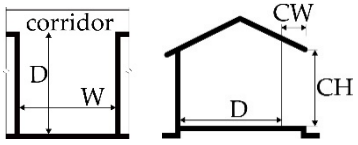
	Zhongting	9.735	5.720	4.300	1.370	
	Houzuo	6.640	7.025	5.005	1.725	
Courtyard	Courtyard 1	10.44	5.85	3.85	-	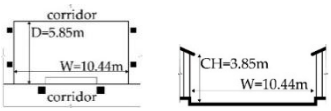
	Courtyard 2	8.85	4.00	5.14	-	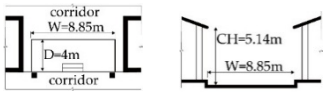

Notes: Dimensions are in m.

3.2. Orientation and Seasonal Analysis

Figure 5 shows the solar path at the location of Wanmu Caotang (113.33° E, 23.17° N). Solar altitudes are higher in summer and lower in winter. The azimuths and times shown

in the diagram are used to interpret differences in direct sunlight exposure between seasons and orientations. A common evaluation period of 07:00–18:00 was used to ensure consistency among simulations.

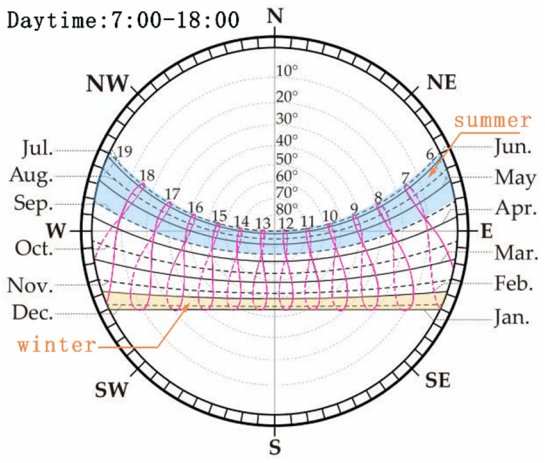

Figure 5. Solar path diagram for Wanmu Caotang.

3.3. Study Prototype and Simulation Configurations

Wanmu Caotang was built in 1804 and subsequently used for teaching as Qiu Clan Study Hall. It is an ancestral hall-type building with a one-axis, three-hall-unit, three-bay layout [32]. Three principal building units and two courtyards are arranged along the longitudinal axis, providing a case for examining mutual shading within a continuous spatial sequence (Figure 6). The dimensions of the entrance (Toumen), central (Zhongting), and rear halls (Houzuo), together with the plan and sectional dimensions of both courtyards, are listed in Table 1. These geometric dimensions were obtained from a new on-site measured survey conducted by the authors for the present study. Building on previous research into the physical environment of Lingnan ancestral halls using Qiu's Ancestral Temple as a case [33], the present study extends the investigation to morphological self-shading through comparisons of indoor direct sunlight and radiative heat gain.

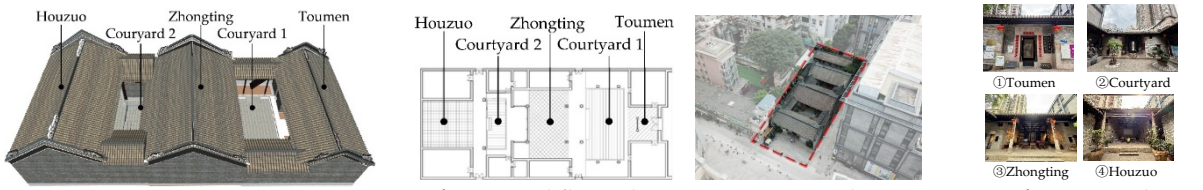

(**a**) Axonometric view (**b**) Ground floor plan (**c**) Aerial view (**d**) On-site photos

Figure 6. Overview and spatial composition of the "Wanmu Caotang" building complex.

Four entrance room–courtyard–main functional room configurations were constructed using the actual room and courtyard dimensions of Qiu Clan Study Hall (the former site of Wanmu Caotang), as obtained from the authors' on-site measured survey described above (Table 2). Configuration A combines the entrance hall (Toumen), courtyard 1, and central hall (Zhongting); B combines the entrance hall (Toumen), courtyard 2, and rear hall (Houzuo); C combines the central hall (Zhongting), courtyard 1, and rear hall (Houzuo); and D combines the central hall (Zhongting), courtyard 2, and rear hall (Houzuo). "Entrance room" refers to the relative position within a modeled combination (Table 2). Thus, the entrance room in C and D is the central hall unit rather than the entrance hall of the actual building.

Table 2. Combinations of building units and courtyards in the four simulation configurations.

Model Name	Entrance Room	Courtyard	Main Functional Room	Plan Layout	Schematic Diagram
Model A	①	Courtyard 1	③	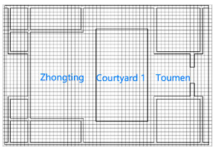	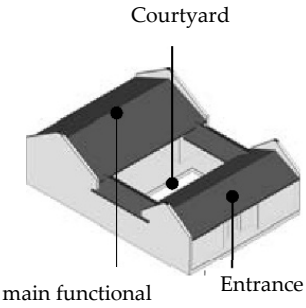
Model B	①	Courtyard 2	⑤	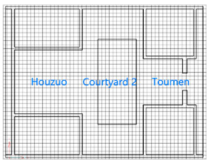	
Model C	③	Courtyard 1	⑤	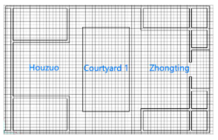	
Model D	③	Courtyard 2	⑤	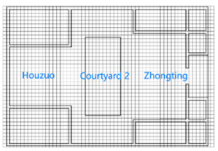	

Room unit ① denotes the entrance hall (Toumen), unit ③ the central hall (Zhongting), and unit ⑤ the rear hall (Houzuo). Combining the configuration letter and room number gives A-1, A-3, B-1, B-5, C-3, C-5, D-3, and D-5. A and B retain the entrance hall while varying the main room and courtyard. B and D retain courtyard 2 and the rear hall while varying the entrance room. Configurations C and D use identical room combinations, enabling comparison of the sunlight and heat-gain responses associated with two overall courtyard geometries.

3.4. Simulation Conditions and Data Processing

SETR was calculated using Ecotect and IRHG using DeST-c, with outputs recorded for each room and orientation in summer and winter. The same indicators were applied to all four configurations. Orientation-specific comparisons, room and eave dimension analyses, and courtyard configuration comparisons were combined to describe sunlight exposure and radiative heat gain for the specified forms.

The Ecotect direct sunlight analysis used an indoor grid with a minimum cell size of 400 mm × 400 mm at a height of 800 mm above the floor. The evaluation period was 07:00–18:00. Sixteen orientations were set at clockwise intervals of 22.5°, starting from north (N).

The thermal transmittances of envelope components in the DeST-c models are listed in Table 3. Natural ventilation was specified, with no air-conditioning, lighting, or indoor shading systems. Openings were represented by 6 mm clear-glass windows. The resulting IRHG represents mean daily solar-related heat gain per room, not air-conditioning electricity consumption. The on-site survey provided geometric inputs. Corresponding field measurements of indoor sunlight exposure and solar-related heat gain were unavailable for direct validation, and sensitivity to alternative opening states, ventilation rates, and shading operation was not quantified. The simulations therefore support comparisons under the stated assumptions.

Data were processed separately for summer and winter. For each season, SETR and IRHG were averaged across the 16 orientations for each of the eight modeled room instances

(N = 8). Pearson correlation coefficients between these room means and the corresponding room and eave dimensions describe associations within the modeled configurations. The eight instances reuse three measured hall-unit geometries. Courtyard comparisons used differences between corresponding rooms in configurations D and C under the same season and orientation (D–C). For each corresponding room and season, the 16 orientation-specific differences were summed and divided by 16 to obtain the arithmetic mean, and the minimum and maximum differences were also reported. For Appendix A, the orientation-mean IRHG for each room was also divided by its reference plan area.

Table 3. Envelope materials and thermal transmittances used in the simulation models.

Component	Material	Thermal Transmittance ($W/(m^2 \cdot K)$)
External and internal walls	Solid clay brick, 300 mm	0.331
Roof	Clay tile, 20 mm + cement mortar, 5 mm + clay tile, 20 mm + pine wood, 20 mm	0.812
Floor	Clay brick, 25 mm + rammed earth, 500 mm	1.670
Opening (modeled as a window)	Clear glass, 6 mm	4.350

4. Results

4.1. Orientation and Seasonal Sunlight Exposure

Figure 7 presents summer and winter SETR and IRHG for each room in the four configurations across orientations. Higher SETR indicates a greater proportion of direct sunlight exposure time at sampling points within the common evaluation period; higher IRHG indicates greater mean daily solar-related heat gain for the entire room. The indicators describe direct sunlight exposure and total room heat gain, respectively. Their orientation patterns can be considered together to analyze the seasonal solar response of the specified ancestral hall forms, but cannot be directly combined into a single ranking of annual self-shading performance.

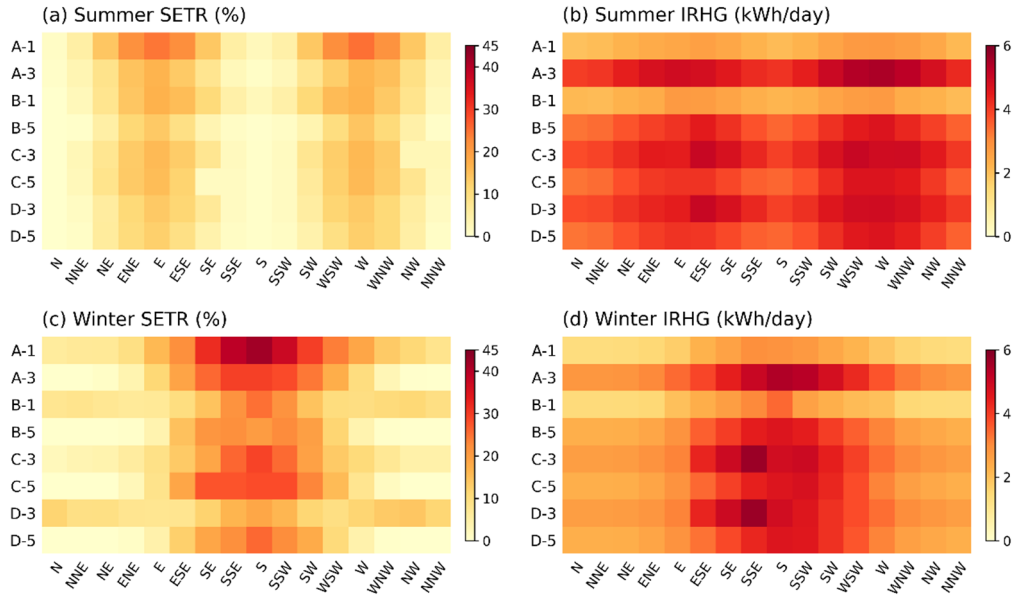

Figure 7. SETR and IRHG for each room across orientations: (**a**) summer SETR (%); (**b**) summer IRHG (kWh/d); (**c**) winter SETR (%); (**d**) winter IRHG (kWh/d).

Summer: Each room's maximum SETR occurs in an easterly or westerly orientation. In A-1, east- and west-facing SETR values are 24.6% and 25.1%, respectively, indicating that the sampling points receive direct sunlight for approximately one-quarter of the 07:00–18:00 evaluation period on average. Other configurations show similar orientation trends but different exposure levels: maximum summer SETR values for B-1, C-3, and D-3 are 17.0%, 16.0%, and 13.6%, respectively. SETR is generally lower in southerly and northerly orientations. Each room reaches its minimum when facing north, with B-5 and D-5 both at 0%. South-facing values also remain low, such as 0.3% in B-5. Thus, all four configurations share a summer pattern of greater direct sunlight exposure in east- and west-facing rooms and lower exposure in south- and north-facing rooms, although values depend on the room and its spatial configuration.

High IRHG values likewise occur mainly in easterly and westerly orientations and nearby directions. Across all summer scenarios, the maximum is 5.45 kWh/d in west-facing A-3 and the minimum is 1.95 kWh/d in north-facing A-1. However, peak heat-gain orientations differ among rooms: C-3 peaks at west-southwest (WSW), whereas D-3 peaks at east-southeast (ESE). Summer SETR and IRHG therefore follow broadly similar orientation trends, but the orientation with the longest direct sunlight exposure does not necessarily have the highest total room heat gain. The two indicators must be assessed separately.

Winter: High SETR values shift from the easterly and westerly orientations observed in summer toward southerly orientations. Due-south-facing A-1 reaches the maximum winter SETR across all scenarios, at 41.8%, meaning that sampling points receive direct sunlight for approximately 40% of the common evaluation period on average. Some rooms peak near, rather than exactly at, due south: A-3 peaks at south-southeast (SSE), while B-5 and C-5 peak at south-southwest (SSW). Winter sunlight maxima should therefore be described as concentrated around southerly orientations rather than uniformly occurring at due south. North-facing exposure is generally low but varies among rooms. SETR is 0% for A-3, B-5, C-5, and D-5, but 6.1%, 7.6%, and 11.9% for A-1, B-1, and D-3, respectively.

Each room's maximum winter IRHG occurs at SSE, S, or SSW. Across all winter scenarios, the maximum is 5.65 kWh/d in SSE-facing C-3 and D-3. Each room reaches its minimum when facing north, with the lowest value of 1.38 kWh/d in A-1. Compared with summer, high exposure ratios and radiative heat gains are more concentrated around southerly orientations in winter. Nevertheless, SETR and IRHG peaks still differ: winter SETR in A-1 peaks at due south, whereas its IRHG peaks at SSE.

Across the two seasons, orientation has a distinct seasonal influence on indoor solar radiation. Averaging equally across the eight modeled rooms, south-facing SETR rises from 0.93% in summer to 27.31% in winter, whereas east- and west-facing SETR falls from 16.15% and 16.28% in summer to 8.46% and 9.59% in winter, respectively. These changes correspond to the seasonal shift in the solar path (Figure 5), demonstrating different exposure characteristics for the same hall–courtyard form in different seasons.

The seasonal roles of orientation in this case can therefore be summarized as follows. North-facing rooms generally maintain low direct sunlight exposure and room heat gain in both seasons. East- and west-facing rooms require particular attention for summer sunlight control. South-facing rooms combine low summer exposure with substantially increased winter exposure. This southerly response illustrates the seasonal contrast between summer sunlight exclusion and winter sunlight access within the specified ancestral hall forms. This pattern describes seasonal sunlight access; the simulations do not establish indoor thermal comfort.

4.2. Effects of Building Dimensions

Room dimensions and eave proportions are associated with direct sunlight exposure and indoor radiative heat gain in the modeled configurations. Using the room and eave

dimensions in Table 1, this section examines their descriptive Pearson correlations with summer and winter SETR and IRHG (Table 4). The geometric diagrams in Figure 8 and simulation results for different rooms are considered together to analyze the relationships of width, depth, and eave proportions with exposure time and total room heat gain, thereby clarifying scale trade-offs in morphological self-shading.

Table 4. Descriptive room-level Pearson correlations between geometric parameters and seasonal orientation-mean SETR or IRHG.

Dimensional Parameter	Summer		Winter	
	SETR	**IRHG**	**SETR**	**IRHG**
Room width, W	−0.440	0.903	−0.278	0.910
Room depth, D	−0.824	0.678	−0.747	0.668
Reference plan area, A_ref	−0.717	0.996	−0.558	0.997
Eave height, CH	−0.498	0.040	−0.534	0.025
Eave projection width, CW	−0.844	0.779	−0.746	0.771
Eave height-to-width ratio, CH/CW	0.826	−0.932	0.692	−0.927

Note: Each correlation uses eight modeled room instances per season (N = 8). One observation is a room's mean across the 16 modeled orientations paired with its corresponding geometry. The eight instances reuse three measured hall-unit geometries.

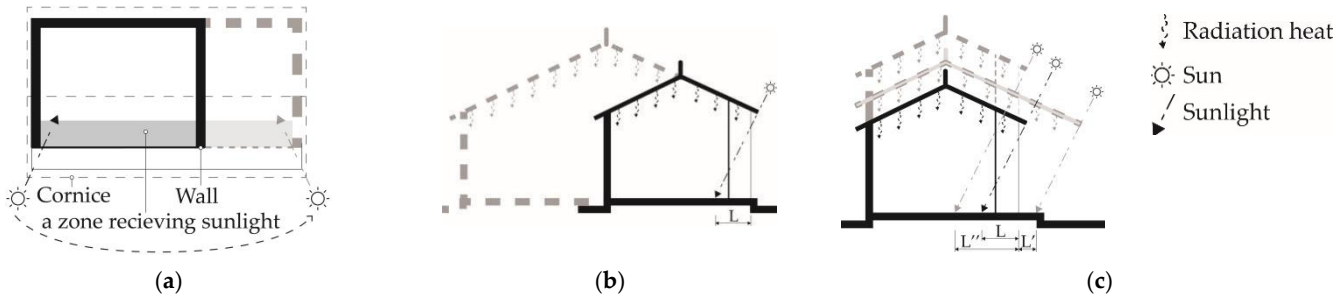

Figure 8. Schematic effects of geometry on sunlight penetration and solar-related heat transfer: (**a**) room width; (**b**) room depth; (**c**) eave height-to-width ratio. The panels illustrate geometric mechanisms.

Room dimensions have different associations with the two indicators. Room width is negatively correlated with SETR, with summer and winter coefficients of −0.440 and −0.278, respectively, but positively correlated with IRHG, at 0.903 and 0.910. Room depth has correlations of −0.824 and −0.747 with SETR, compared with 0.678 and 0.668 with IRHG. Reference plan area has correlations of −0.717 and −0.558 with SETR and 0.996 and 0.997 with IRHG. Among the rooms compared, greater depth generally corresponds to a lower mean exposure time ratio at sampling points, whereas larger room area corresponds to higher total room heat gain. Changes in heat gain associated with increasing room dimensions therefore do not track changes in direct sunlight exposure time.

Eave parameters also show different associations with sunlight exclusion and total room heat gain. Eave width is negatively correlated with SETR in both seasons, with coefficients of −0.844 in summer and −0.746 in winter. The eave height-to-width ratio is positively correlated with SETR, at 0.826 and 0.692. Thus, wider eaves and lower height-to-width ratios generally correspond to shorter exposure times at sampling points, with slightly larger absolute correlations in summer. Meanwhile, eave width is positively correlated with IRHG, at 0.779 and 0.771, whereas the height-to-width ratio is negatively correlated, at −0.932 and −0.927. Correlations between eave height and IRHG are weak within these

configurations, at 0.040 and 0.025. Rooms with wider eaves can therefore have lower SETR without necessarily having lower total room heat gain.

Figure 8 provides a geometric explanation for these differences. Under the simplified conditions illustrated, increasing room width while holding depth, opening configuration, and solar incidence constant mainly expands the lateral extent of the sunlit area without increasing the penetration distance along the room depth. The total area receiving direct sunlight may therefore increase without a substantial change in its proportion of the room area. This helps explain the smaller magnitude of the width–SETR correlation compared with the depth–SETR correlation, although instantaneous sunlit area fraction and mean point exposure time over an evaluation period remain distinct measures. Wider rooms generally have higher IRHG in the room comparisons, indicating that total room heat gain can differ appreciably without a corresponding increase in point exposure time.

For room depth, sunlight penetration remains relatively unchanged when opening conditions and solar incidence are held constant. Increasing depth mainly adds space at the rear of the room beyond the directly sunlit zone. As the proportion of less-exposed interior space increases, the mean exposure time ratio across sampling points may decrease, providing a geometric explanation for the negative depth–SETR association. In these configurations, greater depth also accompanies larger reference plan area and generally higher IRHG. Deeper rooms can therefore exhibit both less direct sunlight exposure and higher whole-room heat gain. The former reflects the regulation of sunlight access by spatial depth, whereas the latter requires consideration of the overall room dimensions and heat-gain conditions.

For eaves, Figure 8c illustrates how changes in projection width and height affect indoor direct sunlight penetration. With other conditions held constant, wider eaves can shorten the penetration distance, whereas higher eaves may allow sunlight to penetrate farther. The combination of height and projection width is therefore an important geometric condition for self-shading. Wider eaves and lower height-to-width ratios correspond to lower SETR in this case, consistent with this obstruction mechanism. In contrast, the positive eave-width–IRHG correlation describes the overall comparison among the existing room–eave combinations: stronger local exclusion of direct sunlight does not necessarily imply lower total heat gain for the room concerned. Local shading by the eaves should therefore be interpreted alongside the overall scale of room heat gain, rather than attributing higher IRHG directly to wider eaves.

Overall, room dimensions and eave proportions show consistent association directions across summer and winter: greater depth, wider eaves, and lower eave height-to-width ratios generally correspond to lower SETR, whereas larger room area corresponds to higher IRHG. Figure 8 helps explain how depth and eaves obstruct sunlight by changing its penetration into the room, while total room heat gain also needs to be interpreted in relation to overall spatial dimensions. The summer comparison illustrates this scale trade-off: A-3 had lower orientation-mean SETR than A-1 (8.45% versus 13.51%) but higher total IRHG (4.652 versus 2.374 kWh/d). Per unit reference plan area, A-3 had lower heat gain (0.0835 versus 0.1211 kWh/(m^2·d)), reversing the heat-gain ranking (Table A1). This comparison does not isolate the effects of individual dimensions, which vary together. Evaluation of morphological self-shading in Guangfu ancestral halls should therefore consider depth, eave proportions, and room area together, assessing both direct sunlight exclusion and overall radiative heat gain to inform comparisons of dimensional combinations.

4.3. Courtyard Configuration and Sunlight Exposure in Adjacent Rooms

Courtyards, surrounding halls, and verandas together form the spatial enclosure of Guangfu ancestral halls. Their geometry affects sunlight penetration through the courtyard

into adjacent rooms. To compare the self-shading performance of courtyard configurations, this section focuses on C and D, which use identical central and rear hall units. Configuration C uses courtyard 1, whereas D uses courtyard 2. Corresponding rooms are compared under the same season and orientation to examine differences in indoor sunlight exposure and radiative heat gain associated with courtyard configuration.

Figure 9 presents orientation-specific differences, calculated by subtracting SETR and IRHG in the central and rear hall rooms of C from those of the corresponding rooms in D. Negative differences indicate lower exposure time ratios or total room heat gain in D; positive differences indicate higher values in D. SETR differences are expressed in percentage points and IRHG differences in kWh/d. Table 5 summarizes the arithmetic mean, maximum, and minimum of the 16 orientation-specific differences for each room. The mean is obtained by summing the 16 differences and dividing by 16, providing an overall comparison across the orientations considered, while the curves identify the orientation dependence of those differences.

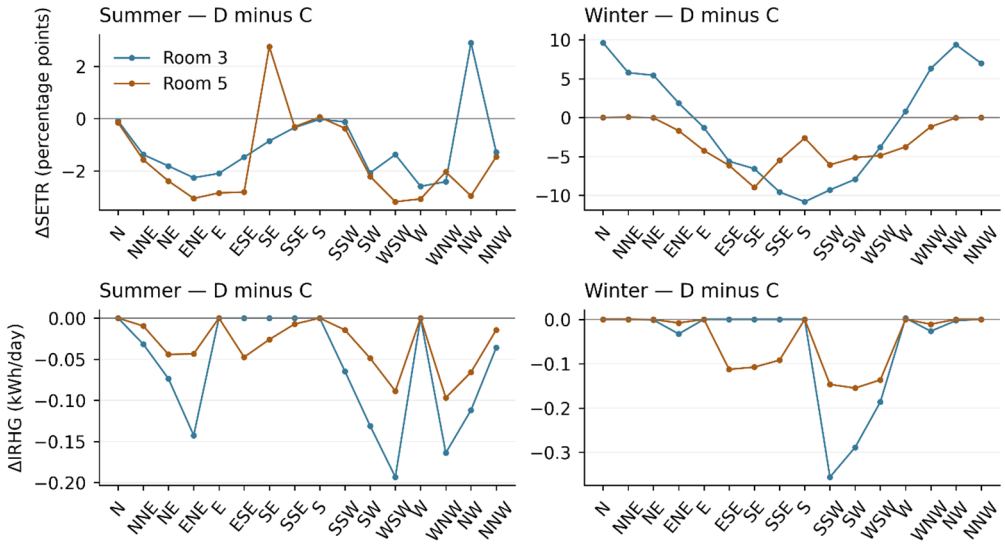

Figure 9. Orientation-specific differences between identical room units in C and D (D–C): upper panels, SETR differences in percentage points; lower panels, IRHG differences in kWh/d. Negative values indicate lower values in D than in C.

Table 5. Mean and range of 16 orientation-specific paired differences between D and C, by room and season (D–C).

Season	Room Unit	Mean ΔSETR (Percentage Points)	ΔSETR Range (Percentage Points)	Mean ΔIRHG (kWh/d)	ΔIRHG Range (kWh/d)
Summer	3	−1.08	−2.59 to +2.90	−0.059	−0.193 to +0.000
Summer	5	−1.60	−3.18 to +2.76	−0.032	−0.097 to +0.000
Winter	3	−0.55	−10.82 to +9.62	−0.056	−0.356 to +0.003
Winter	5	−3.14	−8.98 to +0.06	−0.048	−0.155 to +0.000

Note: Negative values indicate lower values in D. Room 3 is the central hall and room 5 is the rear hall. The maximum winter ΔIRHG for room 5 is approximately +0.000001 kWh/d and rounds to +0.000.

In summer, SETR differences for both the central and rear halls are negative at most orientations, indicating that D generally corresponds to less indoor direct sunlight exposure. Central hall differences range from −2.59 to +2.90 percentage points, with a mean of −1.08 percentage points across 16 orientations. Rear hall differences range from −3.18 to +2.76

percentage points, with a mean of −1.60 percentage points. Thus, both rooms in D have lower orientation-averaged summer exposure ratios, with a larger mean reduction in the rear hall. However, positive differences occur in scenarios such as the northwest-facing central hall and southeast-facing rear hall. The shading advantage of D therefore varies by orientation, and C has lower exposure ratios at some orientations.

In winter, differences between the courtyard configurations depend more strongly on room position. Central hall SETR differences range from −10.82 to +9.62 percentage points, with a mean of −0.55 percentage points. D exceeds C by 9.62 percentage points when facing north but is 10.82 percentage points lower when facing south, demonstrating a reversal between these orientations. Rear hall differences range from −8.98 to +0.06 percentage points, with a mean of −3.14 percentage points; D is lower at most orientations. The mean reduction in rear hall exposure is greater in winter than in summer. Although central hall differences are large at some orientations, positive and negative values offset one another, producing a smaller mean difference. Winter courtyard effects therefore need to be interpreted in relation to room position and specific orientation.

Radiative heat gain results show slightly lower mean IRHG in both rooms of D than in C in both seasons. Mean differences for the central and rear halls are −0.059 and −0.032 kWh/d in summer, and −0.056 and −0.048 kWh/d in winter, respectively. Figure 9 shows that IRHG is similar between the configurations at some orientations, while clearer negative differences occur at others. In orientation-averaged comparisons, D therefore combines lower direct sunlight exposure ratios with slightly lower total room heat gain, although the orientation-specific differences in the two indicators have different magnitudes.

These results can be interpreted in relation to courtyard geometry and enclosure. Courtyard 1 measures approximately 10.44 m × 5.85 m in plan, with an indicated enclosure height of 3.85 m. Courtyard 2 measures approximately 8.85 m × 4.00 m, with an enclosure height of 5.14 m. Configuration D therefore has a smaller courtyard footprint and greater enclosure height. Mutual shading among surrounding halls, roofs, and verandas changes the path of sunlight through the courtyard into adjacent rooms. Geometrically, a more compact enclosure may restrict direct sunlight from certain directions, providing an explanation for lower SETR in most D scenarios. As season and orientation change, the relationship between solar incidence and surrounding obstructions also changes. The central and rear halls occupy different positions in the sequence and experience different shading conditions. This helps explain the winter reversal in central hall differences and the lower rear hall SETR at most orientations. The shading differences should therefore be interpreted through both courtyard plan dimensions and enclosure height, as a comparison of two overall courtyard configurations. Because plan dimensions and enclosure height vary together, this comparison does not isolate the contribution of either parameter.

Overall, with the room combination held constant in this case, configuration D, with its smaller courtyard and greater enclosure height, has lower orientation-averaged SETR in the central and rear halls in both seasons, together with slightly lower mean IRHG. This difference reflects the combined contrast in courtyard plan dimensions and enclosure height. The difference varies by season, orientation, and room position, particularly in the winter central hall, where changes are opposite for northerly and southerly orientations. Courtyard self-shading arises from enclosure formed jointly with surrounding halls and verandas. Relating courtyard geometry to solar incidence and room position thus provides a more specific account of how the Guangfu ancestral hall–courtyard sequence modulates indoor solar radiation.

4.4. Practical Implications and Limitations

Heritage-sensitive assessments consider several kinds of evidence, including how historic character can be reconciled with contemporary use and how risks to existing

buildings can be assessed [34,35]. The present results contribute evidence on seasonal solar exposure and heat gain for the surveyed hall–courtyard sequence.

For the adaptive use of existing heritage buildings, the simulated patterns can inform the choice of rooms and times of use. At Wanmu Caotang, rooms with lower summer direct sunlight exposure could be considered first for activities that require limited exposure to direct sunlight. Where an east- or west-facing room with high summer exposure is needed for a particular use, changes to the schedule or reversible shading measures, such as removable screens, could be assessed on site before permanent alterations are considered. Direct sunlight exposure and total room heat gain should be considered separately when comparing these options, since a room with shorter exposure can still have higher total heat gain.

For new buildings that draw on traditional hall–courtyard layouts, the findings suggest which design choices to test together at an early stage: room orientation, room depth, eave projection, and courtyard enclosure. Where summer shading and winter sunlight access are both desired, candidate layouts can be compared in both seasons. The paired courtyard comparison also shows why plan dimensions and enclosure height should be documented and assessed together. The case findings can guide the choice of design alternatives to test. The study is limited to one surveyed prototype and a small set of modeled configurations. Several room instances reuse the same geometry, and dimensional parameters vary together. As Section 3.4 notes, no corresponding field measurements were available to validate the simulations. Supplementary Data S1 reports SETR and IRHG by room, season, and orientation. These data and the reference dimensions in Table 1 allow readers to reproduce the reported orientation summaries, room-level correlations, paired D–C differences, and reference-area calculations.

5. Conclusions and Future Research

5.1. Main Conclusions

Using Qiu Clan Study Hall (the former site of Wanmu Caotang), Guangzhou, as an ancestral hall-type prototype, this study developed four hall–courtyard configurations and conducted summer and winter simulations across 16 orientations with Ecotect and DeST-c. SETR and IRHG were used to analyze seasonal responses and scale trade-offs in morphological self-shading. The following conclusions apply to the modeled configurations and input conditions of this prototype.

(1) Morphological self-shading exhibits distinct seasonal orientation patterns.

In summer, high direct sunlight exposure occurs mainly in east- and west-facing rooms, with generally lower values in southerly and northerly orientations. SETR in east- and west-facing A-1 is 24.6% and 25.1%, respectively, indicating the importance of these orientations for summer sunlight control in this case. In winter, high exposure and radiative heat gain shift toward southerly orientations, with SETR reaching 41.8% in due-south-facing A-1. Southerly orientations thus combine reduced summer exposure with increased winter sunlight access, illustrating the differential response of the specified hall–courtyard forms to seasonal solar incidence. North-facing exposure is generally low in both seasons, although some rooms still receive direct sunlight in winter.

(2) Scale trade-offs arise from different associations with sunlight exclusion and total room heat gain.

Among the rooms compared, depth and eave width are negatively correlated with SETR in both seasons, whereas the eave height-to-width ratio is positively correlated. Deeper spaces, wider eaves, and lower height-to-width ratios therefore generally correspond to shorter direct sunlight exposure at sampling points. Reference plan area is positively cor-

related with total IRHG, with coefficients of 0.996 in summer and 0.997 in winter. The geometric diagrams explain how depth and eaves obstruct sunlight by changing its penetration into the room, while total room heat gain also relates to overall spatial dimensions and heat-gain conditions. In the summer comparison of A-3 and A-1, lower SETR coincided with higher total IRHG but lower IRHG per unit reference plan area. The scale trade-off therefore depends on whether heat gain is evaluated for the whole room or per unit reference plan area.

(3) The more compact courtyard configuration generally corresponds to lower exposure ratios, with effects varying by season, orientation, and room position.

Configurations C and D use identical central and rear hall units, providing corresponding conditions for courtyard comparison. Both rooms in D, which has a smaller courtyard and greater enclosure height, have lower orientation-averaged SETR than C in summer and winter. The arithmetic mean differences across 16 orientations indicate reductions of 1.08 and 1.60 percentage points in the central and rear halls in summer, and 0.55 and 3.14 percentage points in winter, respectively; mean IRHG is also slightly lower. However, orientation-specific results show that this shading advantage is uneven. Winter central hall differences reverse between northerly and southerly orientations, whereas rear hall SETR remains lower at most orientations. Courtyard self-shading should therefore be understood through plan dimensions, enclosure height, and adjacent room position, reflecting the modulation of indoor solar radiation by the overall hall–courtyard configuration. The paired differences describe the combined change in courtyard plan dimensions and enclosure height.

Taken together, the findings show that, in the Wanmu Caotang prototype, season and orientation shape the overall pattern of indoor sunlight exposure and radiative heat gain, while room and eave geometry and courtyard configuration help explain differences among spaces. Shorter direct sunlight exposure did not necessarily correspond to lower whole-room radiative heat gain, so the two indicators describe complementary aspects of the seasonal solar response of the hall–courtyard layout. For sustainable conservation and adaptive use, the case findings provide a basis for selecting rooms and periods of use and for identifying where additional shading warrants on-site assessment. For new designs informed by traditional hall–courtyard layouts, the case highlights the value of comparing orientation, room and eave dimensions, and courtyard enclosure across seasons while assessing direct sunlight exposure and total room heat gain separately.

5.2. Future Research

This study is based on a single ancestral hall-type prototype and sunlight and radiative heat-gain results under specified simulation conditions. Future work can undertake summer and winter field monitoring and model calibration, combining indoor sunlight distribution, temperature, humidity, and solar-related measurements to test the simulation results further and examine how these morphological characteristics affect conditions during actual use.

For room dimensions and courtyard configurations, future studies can vary depth, eave width, courtyard plan dimensions, and enclosure height separately while specifying room function and controlling other geometric conditions. This would distinguish the roles of individual parameters and their combinations. Particular attention should be given to why courtyard shading differences vary with orientation and room position, extending the present configuration comparisons into testable morphological parameter studies.

For sustainable conservation and adaptive use of Guangfu ancestral halls, future work can also integrate daylighting, ventilation, thermal comfort, and operational energy use to investigate coordination among summer sunlight control, winter sunlight access, and specific use requirements. Additional ancestral hall cases with different combinations of

axes, hall units, and bays can be examined to compare their hall–courtyard sequences and shading characteristics. This would progressively establish the conditions under which the findings apply and provide a stronger basis for environmental improvements that retain traditional spatial forms. Research on thermal comfort, ventilation, and shading in other building types and settings offers methodological context for that work [36–40].

Supplementary Materials: The following supporting information can be downloaded at https://www.mdpi.com/article/10.3390/su182312103/s1, Supplementary Data S1. Complete summer and winter SETR and IRHG data for eight model rooms across 16 orientations.

Author Contributions: Y.P.: Writing—Review & Editing, Supervision, Project administration, Funding acquisition, Investigation, Resources. Y.X.: Methodology, Validation, Formal analysis, Data Curation, Writing—Original Draft, Visualization. Y.Y.: Conceptualization, Methodology, Software, Formal analysis, Writing—Original Draft, Investigation. L.L.: Writing—Review & Editing, Supervision, Project administration, Funding acquisition, Investigation, Resources. W.C.: Investigation, Resources. All authors have read and agreed to the published version of the manuscript.

Funding: This research was supported by the Guangzhou Science and Technology Program (Grant No. 201904010251) and the Natural Science Foundation of Guangdong Province (General Program) (Grant No. 2020A1515011583).

Institutional Review Board Statement: Not applicable.

Informed Consent Statement: Not applicable.

Data Availability Statement: The simulated SETR and IRHG outputs by room, season, and orientation are provided in Supplementary Data S1 (Supplementary_Data_S1.xlsx). The measured geometry, model configurations, and envelope properties are given in Tables 1–3.

Acknowledgments: During the preparation of this manuscript, the authors used ChatGPT (OpenAI; GPT-6.1 Sol) for the purposes of reorganizing existing simulation results, improving their graphical presentation, and checking the manuscript language. The on-site survey, Ecotect and DeST-c simulations, original simulation data, and initial plots were produced by the authors. The authors have reviewed and edited the output and take fully responsible for the content of this publication.

Conflicts of Interest: Yongyi Ye and Weilong Cao are employed by Guangdong Architectural Design and Research Institute Group Co., Ltd. Both authors declare no conflicts of interest related to this work. The remaining authors declare no conflicts of interest.

Appendix A. Reference Plan Area Normalization

Table A1. Mean whole-room IRHG and IRHG per unit reference plan area across the 16 orientations in each season.

Room	Reference Plan Area (m^2)	Summer		Winter	
		IRHG (kWh/d)	q_ref [kWh/(m^2·d)]	IRHG (kWh/d)	q_ref [kWh/(m^2·d)]
A-1	19.608	2.374	0.1211	1.987	0.1013
A-3	55.684	4.652	0.0835	3.797	0.0682
B-1	19.608	2.393	0.1220	2.036	0.1039
B-5	46.646	3.942	0.0845	3.217	0.0690
C-3	55.684	4.458	0.0800	3.692	0.0663
C-5	46.646	3.937	0.0844	3.258	0.0698
D-3	55.684	4.398	0.0790	3.636	0.0653
D-5	46.646	3.905	0.0837	3.209	0.0688

Note: The reference plan area is the measured reference width multiplied by depth. Calculations use unrounded values; only the displayed values are rounded.

References

1. Zhang, M.; Liu, F.; Liu, Q.; Zhang, F.; Li, T. Climate Adaptation Analysis and Comfort Optimization Strategies for Traditional Residential Buildings in Hot-Summer, Cold-Winter Regions: A Case Study in Xuzhou, China. *Sustainability* **2024**, *16*, 3411. [CrossRef]
2. Shou, T.; Xu, H. Climate adaptation in traditional dwelling typologies: The case of Southern Anhui, China. *Archit. Eng. Des. Manag.* **2024**, *20*, 1301–1322. [CrossRef]
3. Xu, J.; Lu, Z.; Gao, W.; Yang, M.; Su, M. The comparative study on the climate adaptability based on indoor physical environment of traditional dwelling in Qinba mountainous areas, China. *Energy Build.* **2019**, *197*, 140–155. [CrossRef]
4. Wang, S.; Fan, W.; Li, D.; Li, P. Extraction and simulation analysis of climate adaptation strategy for raw earth dwellings in the Tumochuan area of China based on the prototype of building space. *J. Asian Archit. Build. Eng.* **2025**, *25*, 5849–5873. [CrossRef]
5. Sari, L.H.; Wulandari, E.; Idris, Y. An investigation of the sustainability of old traditional mosque architecture: Case study of three mosques in Gayo Highland, Aceh, Indonesia. *J. Asian Archit. Build. Eng.* **2024**, *23*, 528–541. [CrossRef]
6. Wan, F.; Li, Z.; Li, H.; Li, L.; Xiao, X. Climate-Adaptive Archetypes of Vernacular Villages and Their Application in Public Building Design: A Case Study of a Visitor Center in Chaoshan, China. *Buildings* **2025**, *15*, 2848. [CrossRef]
7. Rodrigues, L.; Cherian, B.A.; Tokbolat, S. Reducing Cooling Energy Demand in Saudi Arabian Residential Buildings Using Passive Design Approaches. *Buildings* **2025**, *15*, 1895. [CrossRef]
8. Valladares-Rendón, L.G.; Schmid, G.; Lo, S.L. Review on energy savings by solar control techniques and optimal building orientation for the strategic placement of façade shading systems. *Energy Build.* **2017**, *140*, 458–479. [CrossRef]
9. Renuka, S.M.; Maharani, C.M.; Nagasudha, S.; Raveena Priya, R. Optimization of energy consumption based on orientation and location of the building. *Mater. Today Proc.* **2022**, *65*, 527–536. [CrossRef]
10. Chi, F.; Zhang, J.; Li, G.; Zhu, Z.; Dewancker, B. An investigation of the impact of Building Azimuth on energy consumption in sizhai traditional dwellings. *Energy* **2019**, *180*, 594–614. [CrossRef]
11. Zune, M.; Pantua, C.A.J.; Rodrigues, L.; Gillott, M. A review of traditional multistage roofs design and performance in vernacular buildings in Myanmar. *Sustain. Cities Soc.* **2020**, *60*, 102240. [CrossRef]
12. Nasruddin; Alam, A.G.; Sohel, M.I. Optimization of the Building Envelope and Roof Shading to Reduce the Energy Consumption of College Low-Rise Buildings in Indonesia. *Makara J. Technol.* **2023**, *27*, 99–106. [CrossRef]
13. Eskandari, H.; Saedvandi, M.; Mahdavinejad, M. The Impact of Iwan as a Traditional Shading Device on the Building Energy Consumption. *Buildings* **2018**, *8*, 3. [CrossRef]
14. Soflaei, F.; Shokouhian, M.; Abraveshdar, H.; Alipour, A. The impact of courtyard design variants on shading performance in hot-arid climates of Iran. *Energy Build.* **2017**, *143*, 71–83. [CrossRef]
15. Shou, T.; Pan, Y.; Zhao, B. Vernacular ecological construction: A diagrammatic exploration on the composition modes of spatial-landscape in Huizhou courtyard dwellings. *Archit. Eng. Des. Manag.* **2026**, *22*, 446–470. [CrossRef]
16. Kubota, T.; Zakaria, M.A.; Abe, S.; Toe, D.H.C. Thermal functions of internal courtyards in traditional Chinese shophouses in the hot-humid climate of Malaysia. *Build. Environ.* **2017**, *112*, 115–131. [CrossRef]
17. Ernest, R.; Ford, B. The role of multiple-courtyards in the promotion of convective cooling. *Archit. Sci. Rev.* **2012**, *55*, 241–249. [CrossRef]
18. Almhafdy, A.; Ibrahim, N.; Ahmad, S.S.; Yahya, J. Courtyard Design Variants and Microclimate Performance. *Procedia-Soc. Behav. Sci.* **2013**, *101*, 170–180. [CrossRef]
19. Xu, X.; Luo, F.; Wang, W.; Hong, T.; Fu, X. Performance-Based Evaluation of Courtyard Design in China's Cold-Winter Hot-Summer Climate Regions. *Sustainability* **2018**, *10*, 3950. [CrossRef]
20. Xu, Z.; Huang, X.; Zheng, X.; Deng, J.Y.; Sun, B. A Performance and Data-Driven Method for Optimization of Traditional Courtyards. *Sustainability* **2024**, *16*, 5779. [CrossRef]
21. Kirimtat, A.; Koyunbaba, B.K.; Chatzikonstantinou, I.; Sariyildiz, S. Review of simulation modeling for shading devices in buildings. *Renew. Sustain. Energy Rev.* **2016**, *53*, 23–49. [CrossRef]
22. Kirimtat, A. Shading devices in buildings: A systematic up-to-date review across performance evaluation-based methods. *Energy Build.* **2026**, *353*, 116822. [CrossRef]
23. Mellado Mascaraque, M.Á.; Castilla Pascual, F.J.; Pérez Andreu, V.; Gosalbo Guenot, G.A. Evaluation of the Thermal Comfort and Energy Demand in a Building with Rammed Earth Walls in Spain: Influence of the Use of In Situ Measured Thermal Conductivity and Estimated Values. *Buildings* **2021**, *11*, 635. [CrossRef]
24. Wang, J. Analysis and Application of Ecological Strategies in the Bamboo-Tube House, a Traditional Guangfu Dwelling. *Urban. Archit.* **2025**, *22*, 39–42.
25. Chen, J.; Wang, C. Region Adaptability of XiGuan Grand House and Its Value to Ecological Architecture Design. *IOP Conf. Ser. Earth Environ. Sci.* **2020**, *435*, 012032. [CrossRef]
26. Ji, H.; Wu, S.; Ye, B.; Wang, S.; Chen, Y.; Deng, J.Y. Exploring the Implementation Path of Passive Heat-Protection Design Heritage in Lingnan Buildings. *Buildings* **2023**, *13*, 2954. [CrossRef]

27. Fu, Z.; Yu, G.; Zhang, S.; Zhang, Z. A multi-scale semantic segmentation approach for architectural pattern recognition in traditional cantonese ancestral halls. *npj Herit. Sci.* **2025**, *13*, 669. [CrossRef]
28. Guangzhou Weather. Climate Data for Guangzhou. Available online: http://www.tqyb.com.cn/gz/climaticprediction/static (accessed on 29 June 2025).
29. Qu, J.X. A Preliminary Study of the Architectural Form of Guangfu Ancestral Halls. *Beauty Times (Urban Ed.)* **2018**, *7*, 32–33.
30. Yan, D.; Xia, J.; Tang, W.; Song, F.; Zhang, X.; Jiang, Y. DeST—An integrated building simulation toolkit Part I: Fundamentals. *Build. Simul.* **2008**, *1*, 95–110. [CrossRef]
31. Su, J.; Zhang, J.; Li, G.; Zhang, W.; Yu, H.; Kang, L.; Zhang, L.; Zhang, X.; Wang, J. Research on Dynamic Simulation and Optimization of Building Energy Consumption of Substations in Cold Regions Based on DeST: A Case Study of an Indoor Substation in Shijiazhuang. *Buildings* **2025**, *15*, 3706. [CrossRef]
32. Guangzhou Civil Affairs Bureau. Guangzhou Protected Place Names Register (First Batch): Wanmu Caotang Entry. Available online: https://mzj.gz.gov.cn/attachment/7/7537/7537434/8753411.pdf (accessed on 9 October 2026).
33. Pang, Y.; Li, L.; Fang, W.; Zeng, Z. A Study of Creation of Physical Environment of Ancestral Temples in Lingnan—Take Qiu's Ancestral Temple at Guangzhou as example. In *Proceedings of the 5th Annual International Conference on Architecture and Civil Engineering (ACE 2017)*; Global Science & Technology Forum: Singapore, 2017; pp. 456–462. [CrossRef]
34. Drăghici, C.; Onescu, I.; Tănase, I.; Povian, C.M. Towards a More Cohesive and Accessible City Centre: Bridging the Gap Between Historical Identity and Modern Community's Needs—Case Study: Lugoj City, Romania. *Heritage* **2025**, *8*, 396. [CrossRef]
35. Mouaki Benani, M.; Onescu, I.; Draghici, C.A. Seismic Vulnerability Assessment and Risk Mitigation of Historical Buildings in Lugoj City Center, Romania. *Urban Sci.* **2026**, *10*, 524. [CrossRef]
36. Aqilah, N.; Rijal, H.B.; Zaki, S.A. Indoor thermal environment and effect of air movement on comfort temperature in Malaysian naturally ventilated dwellings. *J. Build. Eng.* **2025**, *104*, 112151. [CrossRef]
37. Hosham, A.F.; Kubota, T. Effects of Building Microclimate on the Thermal Environment of Traditional Japanese Houses during Hot-Humid Summer. *Buildings* **2019**, *9*, 22. [CrossRef]
38. Zhu, L.; Wang, B.; Sun, Y. Multi-objective optimization for energy consumption, daylighting and thermal comfort performance of rural tourism buildings in north China. *Build. Environ.* **2020**, *176*, 106841. [CrossRef]
39. Suhendri; Koerniawan, M.D. Investigation of Indonesian Traditional Houses through CFD Simulation. *IOP Conf. Ser. Mater. Sci. Eng.* **2017**, *180*, 012109. [CrossRef]
40. Yin, S.; Wang, F.; Xiao, Y.; Xue, S. Comparing cooling efficiency of shading strategies for pedestrian thermal comfort in street canyons of traditional shophouse neighbourhoods in Guangzhou, China. *Urban Clim.* **2022**, *43*, 101165. [CrossRef]

Disclaimer/Publisher's Note: The statements, opinions and data contained in all publications are solely those of the individual author(s) and contributor(s) and not of MDPI and/or the editor(s). MDPI and/or the editor(s) disclaim responsibility for any injury to people or property resulting from any ideas, methods, instructions or products referred to in the content.